Sādhanā (2023)48:17
https://doi.org/10.1007/s12046-022-02070-3

Dimensional optimization and modelling of a novel double-ended-tuning-fork micro-resonator for high frequency applications

ANSHU SHARMA[1,*], HARSIMRAN JIT KAUR[2] and VIJAY KUMAR[3]

[1]Chitkara University Institute of Engineering and Technology, Chitkara University, Baddi, Himachal Pradesh, India
[2]Chitkara University Institute of Engineering and Technology, Chitkara University, Rajpura, Punjab, India
[3]MEMS Fabrication Division, Semi-Conductor Laboratory, Government of India, Ajitgarh, Punjab, India
e-mail: anshu.sharma@chitkarauniversity.edu.in

MS received 7 October 2022; revised 20 December 2022; accepted 24 December 2022

Abstract. Micro-resonators are used intensively in various sensors and actuators. An important consideration for resonator-based structures is to have a great level of balance and stability in the vibrational mode opted for resonator operation. In this paper, the object of study is a double-ended-tuning-fork (DETF) resonator which has the inherent advantages of high sensitivity and improved performance. A systematized evaluation of resonator performance is done through a simulative approach for the basic shapes of DETF resonators found in the literature. The boundary organization and geometric framework of the DETF resonator are extensively examined. Resonator modelling is done using the finite element model tool COMSOL and a novel design of the DETF resonator is presented. The focal point of this study is designing a flexural resonator structure suitable in high frequency design requirements along with improved stress considerations for the resonator design. This study demonstrates the outcomes of simulations like impact on stress at the fixed ends, impact on the anti-symmetric mode of operation like its position, frequency, and modal interference. Lastly, certain simplified design rules for novel micro-DETF resonator designing are also presented.

Keywords. Resonator; flexural; tuning fork; anti-symmetric mode; stress; resonant frequency.

1. Introduction

Resonant sensors inherit the utilities of quasi-digital output, very good resolution, stability and improved sensitivity [1, 2]. Further, micro-machining techniques aid in size, weight and cost reduction making the structures more portable and affordable [3]. The key component in a micro-resonant sensor is a micro-resonator whose design optimization is very crucial for achieving optimum device performance [4]. Amongst different types of resonators, flexural resonators are the ones that are highly suited for sensing applications such as sensing pressure [5], force [6], temperature [7] and acceleration [8]. This is due to their inherent low mechanical stiffness [9]. Flexural resonators due to their less stiffness, also have low frequencies. Further due to their large surface to volume ratio, flexural resonators experience higher energy loss from surface effects [10].

A key factor that needs optimization for improved device performance is the amount of energy lost from the vibrating resonator element into the ambient structures [11]. Now, for achieving a high Q factor, the energy coupled from the resonator into the ambient structures should be minimal and reduction in coupled energy necessitates that the resonant frequency should be high [12]. High operational frequencies are also highly desirable in wireless communication [13], biomedical applications [14] and aviation [15]. For increasing the vibrational frequency, the stiffness of a resonator should be higher. Since flexural resonators are intended for usage in sensing applications, an increase in stiffness can pose difficulty since sensitivity decreases with increased stiffness [9]. However, with suitable design optimization it is possible to achieve an improved resonator design along with high frequency operation as has been elaborated in this paper.

The study presented here investigates the results for analysis of flexural resonator in order to introduce a novel flexural resonator design. For selection of appropriate boundary conditions and favourable vibrational model, the resonator selected as object of study is a double-ended tuning fork (DETF). For achieving optimized performance, geometrical boundary of DETF resonator should be chosen such that Q factor achievable is high [11]. For obtaining optimized geometric parameters, it must be well understood how the geometry impacts resonator performance. Different geometric parameters affect operation in different manner

*For correspondence
Published online: 21 January 2023

and obtaining this information is a must to derive the most appropriate structural parameters.

Efficient performance often requires trade-offs between parameters to be taken care off for achieving optimal solution for resonator operational behaviour. In this study impact of various geometric parameters like length, width, thickness of tines, gap between tines, etc. on resonator performance (frequency, stress) is analysed. This paper also presents and discusses the results pertaining to resonator optimization (addition of suspension and additional beams) obtained from finite element software COMSOL. The paper intends to present a modification in flexural DETF resonator design to increase its stiffness and hence increases the operational frequency without compromising with the operational sensitivity.

2. Design considerations

Design optimization is very crucial for reduction in coupled energy. When the coupled energy is less, then following advantages are ensured for the resonator operation: high Q factor, high resolution, immunity to vibrations in environmental components and improved long-term drift [16]. Two factors are very crucial to reduce the amount of energy coupled into the surroundings [17]:

- Optimized resonator design
- Selection of operational mode

For a conventional individual beam clamped at roots shown as resonator A1 in figure 1, the amount of energy dissipated from the anchoring end to the surroundings depends on the anchor. Thus, the stability of natural frequency is difficult to achieve in such resonators. DETF resonators design which include two individual beams clamped at roots, can be very useful to overcome this drawback [19]. The basic resonator designs existing in literature studied in this paper to devise a new improved resonator design are depicted in figure 1 as resonator A2-A6. A variation in resonator A6 shown as resonator A7 in figure 1 was also studied in this paper. A labelled schematic for DETF resonator lying in XY plane is shown in figure 2.

The basic design of DETF resonator as shown in resonator A2 comprises of two fixed-fixed beams (referred to as tines) coupled together at some gap via a fixed base. The structure can be modified by addition of outriggers on both fixed bases as is shown in resonator A3. Another modification incorporated is addition of stubs in both resonators A2 and A3 as is depicted in resonator A4 and A5. Based on the analysis detailed later in the paper, resonator A5 was found to be more suitable for further modification. Thus, suspensions were added to it as is depicted in resonator A6 (two-line suspension) and A7 (three-line suspension). Analysis and results for all the structures along with DETF resonator design that has been modified to achieve the novel desired design are described later in this paper.

Tuning fork based flexural resonators are highly stable and suitable for obtaining high-Q frequency selectivity with dynamically balanced operational mode [20]. The compensating factor for energy loss in tuning fork design is the fact that when two parallel beams vibrate symmetrical and antiphase to each other, then vibrational forces and moments cancel each other. This eliminates any force at the base, trapping vibrational energy inside resonator and thus, high Q factor is achievable [19, 21]. Thus, lateral anti-phase symmetric (AS) mode of operation in which the two tines vibrate in opposite direction is the desired mode for DETF operation. The vibrational mode shape for AS mode is shown in figure 3.

Optimum mode is the one that exhibits least stress values at the fixed ends for the resonator [22]. Lateral vibrational modes are benefitted by the fact that in sensing applications the lateral motion is perpendicular to the motion of substrate beneath the resonator and this reduces the coupled energy, aiding in high Q factor [23]. The lateral AS vibration mode is the desired mode for DETF operation since mechanical coupling is highly reduced when the resonator vibrates, parallelly to the substrate below [24].

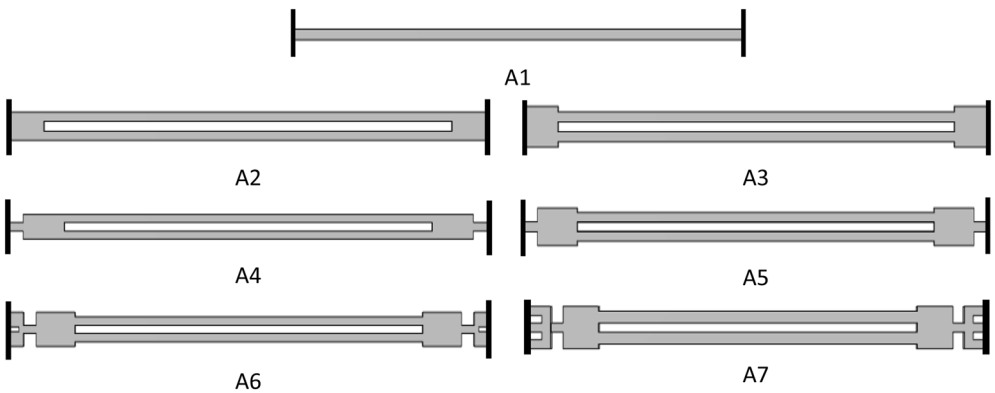

Figure 1. Top view of basic DETF resonator shapes.

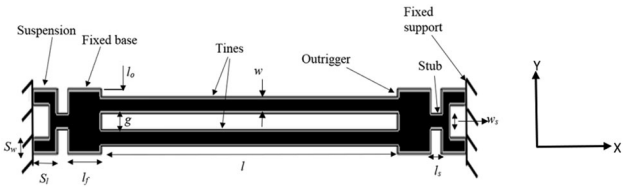

Figure 2. Basic DETF resonator schematic.

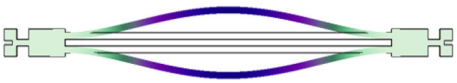

Figure 3. AS mode of vibration.

Further, to reduce coupled energy the design should also aim to increase the resonant frequency ratio of resonator and supporting structure. Thus, to effectively reduce the coupled energy to the substrate, the resonant frequency of the resonator should be made higher [11].

Another important factor is the occurrence of interference modes. All the other modes which exhibit nearby frequencies to the operational mode act as the spurious/interference modes. These are excited if the selection of device geometry is poor, fabrication is asymmetrical and the loading of DETF tines is unequal. A part of vibrational energy of resonator's optimum mode can lead to excitation of these modes. Sensitivity of all these is distinct for the axial load and their existence can even result in cessation of the operation at the desired mode. A proper selection of the ratio between tine width (w) and height (h) helps in realization of interference-mode-free DETF resonator [25, 26].

2.1 *Analytical model for DETF resonator*

In anti-symmetric mode of vibration, due to 180° out of phase movement of tines, a DETF resonator experiences almost negligible displacement at its fixed ends which reduces energy dissipation [27]. Thus, the two tines of DETF resonator can be considered as independent fixed-fixed resonant beams. As per Euler-Bernoulli beam model, for a beam vibration, the dynamic response is managed by the following momentum equation given below [28]–[30]:

$$\frac{\partial^2}{\partial x^2}\left(EI\frac{\partial^2 u(x,t)}{\partial x^2}\right)+\frac{\partial}{\partial x}\left(F\frac{\partial u(x,t)}{\partial u}\right)+\rho A_S\frac{\partial^2 u(x,t)}{\partial t^2} = P_f(x,t) \tag{1}$$

where $u(x,t)$ is the deflection in y direction, x is distance along beam from fixed end, and t is the time. I is second moment of inertia while E and ρ are material properties termed as young's modulus and density respectively. F is the external axial load, A_S is the cross-sectional area of resonant beam and $P_f(x,t)$ is the driving force per unit length.

For a fixed-fixed resonant beam the boundary conditions are as follows:

$$u(x,t) = u(l,t) = 0\left.\frac{\partial u}{\partial x}\right|_{x=0} = \left.\frac{\partial u}{\partial x}\right|_{x=l} = 0 \tag{2}$$

where l is the length of resonating beam.

With the aid of mode superposition theorem, the partial differential equation specified in equation (1) can be decomposed into a combination of various ordinary differential equations. The vibration mode of the beam can be defined as the sum of the mutually orthogonal modes and thus *u (x, t)* can be expressed as

$$u(x,t) = \sum_m \emptyset_m(x) y_m(t) \tag{3}$$

where $\emptyset_m(x)$ represents m order mode shape function of the resonating beam and $y_m(t)$ represents the generalized co-ordinates corresponding to the m^{th} mode. Here, the solution for m^{th} vibration mode can be obtained as

$$M_{e,m}\ddot{y}_m + k_{e,m}y_m = 0 \tag{4}$$

where the k_e and M_e are the effective stiffness and effective mass for a resonating beam with mode m and are expressed as follows.

$$\begin{cases} k_{e,m} = \int_0^l EI\left(\frac{\partial^2 \emptyset_m}{\partial x^2}\right)^2 dx + \int_0^l F\left(\frac{\partial \emptyset_m}{\partial x}\right)^2 dx \\ M_{e,m} = \int_0^l \rho bh \emptyset_m^2 dx \end{cases} \tag{5}$$

Now the general formula for vibrational natural frequency of the resonator is given by expression [3] given in equation (6)

$$f = \frac{1}{2\pi}\sqrt{\frac{k}{M}} \tag{6}$$

where k is the effective stiffness and M is the effective mass of the resonator.

For a DETF resonator, the axial load is equally distributed between its tines as they are basically two parallel fixed-fixed beams. The natural resonant frequency f_0 for the lateral AS mode of vibration for a DETF resonator can be expressed as given in equation (7), [31]. When an axial force F acts upon DETF tines, then the expression for resonant frequency f_r is obtained by equation (8), [31].

$$f_0 = \frac{1.027w}{l^2}\sqrt{\frac{E}{\rho}} \tag{7}$$

$$f_r = f_0\left(1+\frac{0.147l^2}{Etw^3}.F\right) \tag{8}$$

where l , w, t are length width and thickness of the tine.

3. FEM simulations for resonator selection

The design analysis and optimization start with basic geometries of DETF and then certain modified DETF resonator structures are discussed. Selection of proper boundary conditions for a DETF resonator is done by optimizing the resonator geometry for its various dimensional parameters like length, width, height, gap, etc. Geometric optimization and analysis of the resonators were carried out using finite element analysis tool COMSOL. In FEM simulations, isotropic single crystal silicon is chosen as the resonator material. Geometric parameters chosen for the tines are l = 800 μm, w = 10 μm, h = 20 μm and basic gap g in DETF is 10 μm. Boundary structures guidelines for the basic DETF resonators shown in figure 2 are chosen based on the geometric guidelines obtained from literature [18] and are stated in table 1.

The desired mode of operation is chosen based on the stress analysis at the base of fixed tines. Stress at fixed ends is also detrimental for achieving high Q values [32]. High stress value indicates that the mode is out of balance and resonator experiences high energy loss. This implies increased mechanical energy coupling between resonator and surrounding structures and reduced Q values. Therefore, desired mode of operation is one which incorporates least stress at the resonator fixed ends and thus, ensures higher Q values. Further, when a vibrational mode is chosen as the operational mode, then it is highly desirable to keep the spurious modes away from the operating mode so that they have little impact on the working mode [16].

The specific resonant frequency, position of optimum modes and stress values of the optimum vibrational mode for basic DETF resonator designs included in this study are shown in table 2. It can be observed from table 2 that for resonator A2 and A3 stress is very high and frequency difference between modes (modal difference) is very small. Though, with addition of stubs the frequency difference is improved in resonator A4 but stress at the fixed ends is high. Stress was considerably reduced when outriggers were also included as depicted in resonator A5. Then, with the addition of two-line suspension, the stress at the fixed ends became minimal in resonator A6. It became nearly zero with a value of 0.288 N/m^2.

It is known that desired mode of operation should occur at lower vibrational mode of resonator [12]. It was observed in simulation that anti-symmetric mode occurred as mode 2 and from table 2 it can also be seen that mode 1 acts as the interference mode. Table 2 shows that with a frequency difference value of 27.04 kHz, gap between interference and working mode is maximum for resonator A6. A three-line suspension case of resonator A7 was also analyzed. From table 2 we can see that resonator A7 has reduced stress and comparatively good modal frequency difference though these results were better for two-line suspension case (resonator A6). *Hence DETF resonator design chosen for further design modifications is resonator A6.* The basic DETF resonator A6 was analysed to study the impact of geometric variations. Further, the dimensions for length, width, height and gap of tines, suspensions, stubs and outriggers were all varied for resonator A6 using FEM simulations. The evaluated effects on resonator performance are presented in this section.

3.1 *Dimensional optimization for DETF design existing in literature*

Geometric parameters of DETF resonator greatly impact the general behaviour of resonator operation. To evaluate the optimised values for geometric dimensions, various modal analysis simulations were conducted via COMSOL software. The simulative results depicting effects of dimensional variations are shown in figures 4 and 5. It was analysed how the geometry impacts frequency of AS mode, difference between operational mode (AS) frequency from its adjacent nearby modes and stress at the fixed ends of resonator for determining the optimum mode position. The results derived from simulation are discussed here in this section and final dimensions chosen for DETF resonator that is to be further modified are tabulated in table 3.

Table 4 shows the simulated schematics for the first six vibrational modes of the basic DETF resonator along with their frequencies and stress at the fixed ends. It can be seen that the mode with least stress value occurred at second mode and it is the AS mode.

3.1a *Impact of geometric variation on frequency of AS mode and difference between AS mode frequency from its adjacent nearby mode:* Impact of variation in resonator's geometric parameters such as dimensions of tines, stubs, suspensions and outriggers was evaluated via simulations. Simulated values for the frequency of AS mode and its gap from the frequency of nearest adjacent mode are plotted on graphs as shown in figure 4(a-h). It can be seen from graphs in figure 4(a-h) that amongst different geometric variables,

Table 1. Boundary structure guidelines for DETF geometric boundary.

For the beam/tine of length l, width w, thickness h, and gap g	Outrigger width, (l_o)	Fixed base length, (l_f)		Stub length, (l_s)	Stub width, (w_s)
		Without stubs	With stubs		
	$l_o = \frac{g}{2}$	$l_f = \frac{l}{12}$	$l_f = \frac{l}{9}$	$l_s = \frac{l}{27}$	$w_s > \frac{w}{10}$

Table 2. Simulated parameters for basic six resonators.

Resonator	Optimum mode position		Frequency (Hz)	Stress at fixed end (N/m^2)		Mode 1 frequency (Hz)	Mode 2 (AS) frequency (Hz)	Frequency difference (kHz)
				Optimum mode	AS mode			
A2	2	AS	1.3436e5	42.845	42.845	1.3161e5	1.3436e5	2.75
A3	2	AS	1.3519e5	24.655	24.655	1.3419e5	1.3519e5	1 .00
A4	6		3.6994e5	22.602	118.08	1.1364e5	1.3443e5	20.79
A5	2	AS	1.3517e5	2.986	2.986	1.1368e5	1.3517e5	21.49
A6	2	AS	**1.3512e5**	**0.288**	**0.288**	1.0808e5	1.3512e5	**27.04**
A7	2	AS	1.3516e5	3.798	3.798	1.1259e5	1.3516e5	22.57

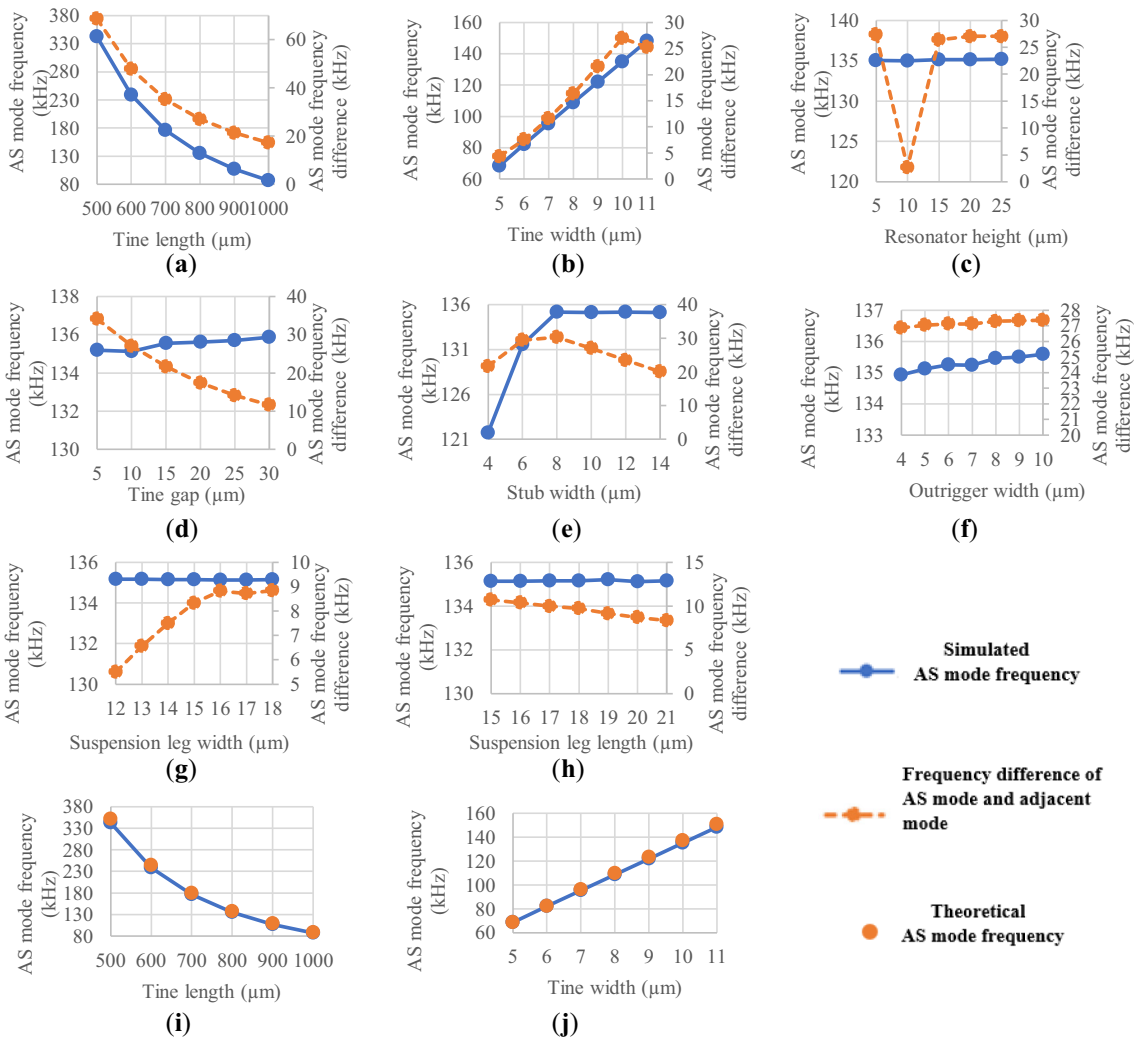

Figure 4. Impact on AS mode frequency and its frequency difference with adjacent mode with variation in (a) tine length, (b) tine width, (c) resonator height, (d) tine gap, (e) stub width, (f) outrigger width, (g) suspension leg width, (h) suspension leg length; Theoretical vs Simulated values for resonant frequency of AS mode w.r.t. variation in (i) tine length of the resonator and (j) tine width of the resonator.

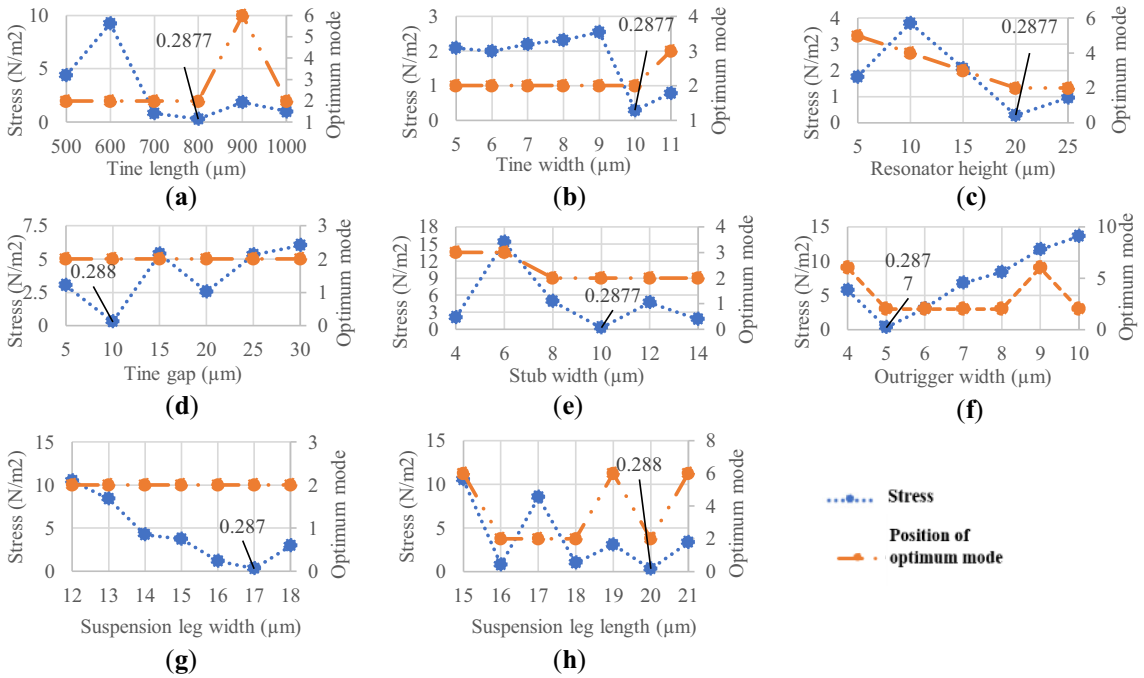

Figure 5. Impact on stress at fixed ends of tines and position of optimum mode for tine vibration with variation in (a) tine length, (b) tine width, (c) resonator height, (d) gap between tines, (e) stub width, (f) outrigger width, (g) suspension leg length and (h) suspension leg width.

Table 3. Dimensions selected for DTEF resonator to be modified.

Resonator boundary parameter dimensions (μm)										
					Fixed base		Stub		Suspension	
Tine length (l)	Tine width (w)	Resonator height (t)	Tine gap (g)	Outrigger width (l_o)	Length (l_f)	Width (l_w)	Length (l_s)	Width (w_s)	Length (S_l)	Width (S_w)
800	10	20	10	5	88.89	40	29.63	10	20	17

Table 4. Characteristics of vibrational resonant modes of DETF resonator.

Vibration mode position	Resonant vibrational mode schematic	Mode type	Stress at fixed ends (N/m^2)	Resonant frequency (Hz)
1		Lateral	1211.4	1.0808e5
2		Lateral	**0.28770**	**1.3512e5**
3		Transverse	8630.9	1.4384e5
4	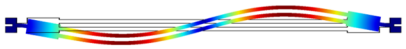	Lateral	4756.7	2.1177e5
5		Transverse	1339.0	2.6080e5
6	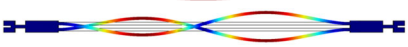	Lateral	1.0417	3.7220e5

only length and width of the tine impacts AS mode frequency. This effect can also be verified theoretically using the formula given in equation (7). Figure 4(a-h) also shows that all the geometric variables except outrigger width l_o, have an impact on the frequency gap between AS mode and its nearby adjacent mode. The simulated AS mode frequency values are all validated theoretically and their variation w.r.t. variation in length and width of tine are shown in figure4(i-j).

3.1b *Impact of geometric variation on position of optimal mode and stress at tine ends:* It is known that for a vibrating element all the modes of vibration are present at a moment

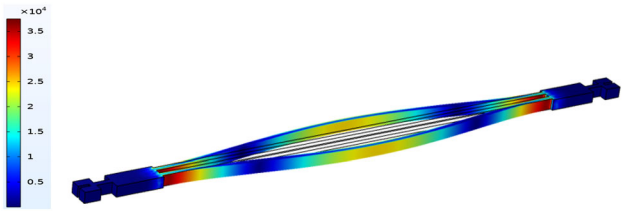

Figure 6. Stress profile schematic of basis DETF resonator A6.

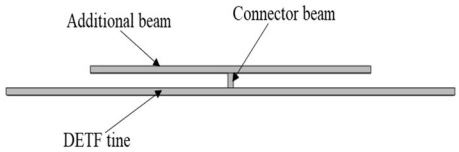

Figure 7. Schematic for modification done with DETF tine of basic resonator.

and hence it is desired to have operational mode at the lower order mode. The simulations showed that for lateral AS mode to occur at a lower position of vibrational operation, a ratio of 1:2 must be maintained between width and height. Geometric optimization carried out in this study enabled occurrence of optimal AS mode at 2nd mode position as is depicted in figure 5(a-h). Evaluation of the stress at fixed ends via simulation showed a minimum value of 0.288 N/m^2 for resonator height of 20 μm, tine length of 800 μm and tine width of 10 μm as is shown in figure 5(a-c). Thus, tine dimensions of 800 μm X 10 μm X 20 μm, were chosen where stress at fixed ends was minimum and modal difference was optimum. Gap between tines and stub width diversely impact the stress at the fixed ends as can be observed in figure 5(d, e). It is observed that for a tine gap of 10 μm the stress is minimum and it maintains that value when stub width is kept equal to the gap between tines. Choice of outrigger region width does impact stress at fixed ends and is minimal when it is half of the gap between tines as is depicted in figure 5(f). Further, increase in suspension width decreased the stress at fixed ends as can be seen in figure 5(g). For a width of 17 μm, variation in length of suspension showed that the stress at the fixed ends varies non-uniformly and was minimum for 20 μm length as is inferred from figure 5(h). A simulated stress profile for the resonator A6 is depicted in figure 6. It shows that maximum stress is at the tine ends and stress is minimal at the fixed ends.

4. Analysis of proposed novel structure

A modified geometry for DETF resonator is analysed, improvised and compared with basic DETF geometry of resonator A6 and the modification done is depicted in figure 7. An additional beam was added with a connector beam placed at the centre of the DETF tine. It has been stated earlier in the paper that a high frequency resonator operation is highly desirable. The aim of the modification done is to achieve a DETF resonator design with high resonant frequency in comparison to basic DETF resonator. The structure with additional beams was analyzed for both non-fixed and fixed ends of the additional beam. Figure 8(a) depicts the schematic for DETF resonator with additional beam whose ends are non-fixed (NFR) and figure 8(b) depicts the case where ends are fixed (FR). Their respective lateral AS mode of operation are shown in figure 9(a, b) respectively. Figure 9(a) shows that the entire additional beam experiences the same maximum displacement as that of the centre of the tine in resonator NFR. Figure 9(b) shows that for resonator FR, only the centre of the additional beam experiences the same maximum deflection as that of the tine centre.

4.1 *Analytical model for proposed DETF resonator*

Based on the analytical model presented in section 2, the equation for flexing of beam can be used here as well. The value for effective mass is attributed to the contribution of added mass m_a, owing to inclusion of additional beams to the DETF tines. Thus, the effective mass in equation (5) is now deduced as follows [32]:

$$M_{e,m} = \int_0^l \rho bh \emptyset_m^2 dx + m_a \emptyset_m(x_a)^2 \tag{9}$$

The resonator considered here is of height h with tines of length l and width w, additional beams of length l_a and w_a and connector beams of length l_c and width w_c. When subjected to a point load at centre, the elastic curve of the clamped-clamped beam in AS mode can be approximated by the mode shape function $\emptyset_m = \emptyset_2 = 16\varepsilon^3 - 12\varepsilon^2 + 1$ with $\varepsilon = \frac{x}{l}$ [33]. Thus, under the influence of equation (9) the expression for effective mass for the modified resonator design in AS mode is as follows [30]:

$$M_e = \rho h\left(\frac{13}{35} wl + w_c l_c + w_a l_a\right) \tag{10}$$

Based on the vibrational shape of the AS mode, the values for the effective stiffness for the resonator NFR and FR can be obtained as follows. As has been stated earlier, the two tines of the DETF act as independent fixed-fixed beams, thus the stiffness of the resonator NFR is the stiffness of a simple beam fixed at both ends [34, 35]. Thus, the expression for effective stiffness k_{en} is as follows:

$$k_{en} = \frac{192Eh}{12} \cdot \frac{w^3}{l^3} \tag{11}$$

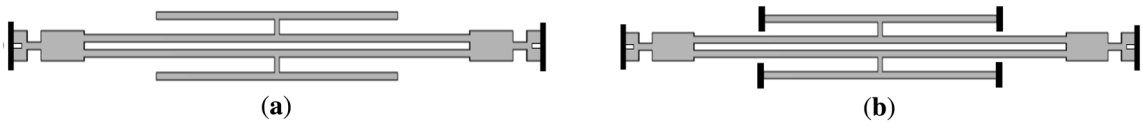

Figure 8. Basic DETF resonator with (a) non-fixed additional beams, (b) fixed additional beams.

Figure 9. Lateral AS mode for DETF with additional beams whose ends are (a) non-fixed, (b) fixed.

According to the structure of the resonator FR, the effective stiffness k_{ef} can be evaluated as

$$k_{ef} = k_b + k_a \tag{12}$$

Where k_b and k_a are the stiffness attributed by the DETF tine and additional beam. Further the very fact that the DETF resonator exhibits two-fold symmetry allows one quarter of the structure to be analyzed [27]. The DETF tine and additional beams thus act as beams having one end fixed and another end being moveable. Hence the effective stiffness of the proposed resonator is as follows [35, 36]:

$$k_{ef} = 4Eh\left(\frac{w^3}{l_1^3} + \frac{w_a^3}{l_2^3}\right) \tag{13}$$

where l_1 and l_2 are the half lengths of DETF tine and additional beam, respectively.

Based on above analysis the natural resonant frequency, $f_{r,m}$ for the lateral AS mode of vibration in the DETF resonators: NFR and FR can thus be expressed as given in equation (14)

$$f_{r,m} = \frac{1}{2\pi}\sqrt{\frac{k_e}{\rho h(\frac{13}{35}w_t l_t + w_c l_c + w_a l_a)}} \tag{14}$$

Depending on the boundary conditions the value of effective stiffness, k_e can be substituted in equation (14) from equations (11) and (13) and corresponding resonant frequency can be evaluated.

4.2 *Dimensional optimization for proposed DETF design*

The dimensions of connector beam were optimized to reduce the stress at the ends of resonator. A connector length of 20 μm and width of 9.9 μm with a fixed additional beam of length 500 μm yielded minimum stress with the value approaching nearly zero. In an attempt to increase the frequency of the flexural resonator design based on DETF resonator, both the designs for additional beams were analyzed for variation in the geometric parameters of the additional beam. The results for AS mode frequency are shown in figure 10(a-c) and that for stress and occurrence of optimum mode are shown in figure 10(d-f).

In figure 10(a, b), it can be seen that with additional beams, the AS mode frequency decreases with increase in length of additional beam for both the structures. Figure 10(c) shows that the variation in AS mode frequency for variation in width of resonator FR. It can also be seen in figure 10(a, b) that for resonator NFR, the AS mode frequency values are far less than that for resonator FR. Figure 10(d, e) shows that the value for stress at the ends in resonator NFR is much greater than the value of 0.80879 N/m^2 for resonator FR. This minimum value is obtained at a length of 500 μm in resonator FR. Thus, resonator FR was chosen for further analysis and the impact of variation in beam width was studied for it only as is depicted in figure 10(c, f). It can be seen that the width of additional beams has very less impact on modal difference and position of optimum mode. The AS mode frequency, however, increases with an increase in width of the additional beam. The optimized value of width is 10 μm for which minimum stress is obtained.

The AS mode frequency of resonator NFR is 81.278 kHz which is much less than the value of 135.12 kHz shown in table 2 for basic DETF resonator A6. This result can be culminated from equation (6) that an increase in mass of the resonator with inclusion of additional beam decreased the frequency. However, in comparison to basic DETF resonator A6, resonator FR exhibited a higher AS mode frequency of 235.96 kHz. Here, the stiffness of the resonator increased by fixing the ends of the additional beam and thus increased the frequency. Simulated stress profiles obtained for the both resonators are shown in figure 11. Figure 11(a) shows that in resonator NFR, there is no stress in the additional beams while figure 11(b) shows that additional beams exhibit stress in resonator FR. Comparing

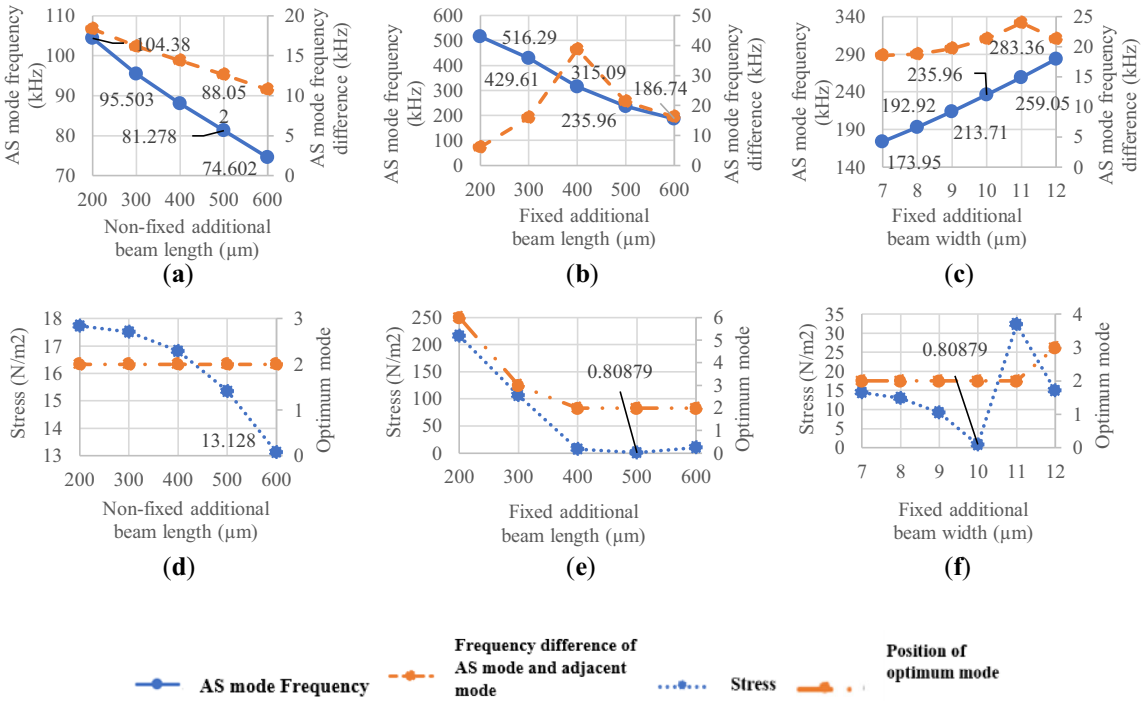

Figure 10. Impact on AS mode frequency and its frequency difference with adjacent mode (a) length (non-fixed ends), (b) length (fixed ends), (c) width (fixed ends); Impact on stress at fixed ends of tines and position of optimum mode for tine vibration for variation in additional beam, (d) length (non-fixed ends), (e) length (fixed ends) and (f) width (fixed ends).

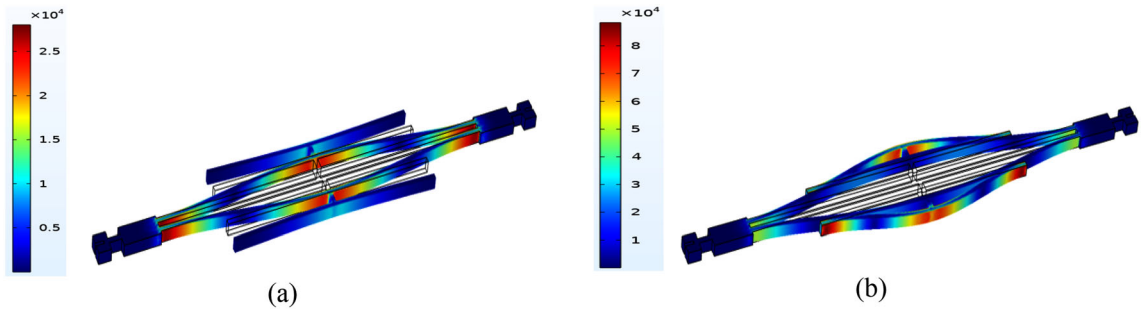

Figure 11. Stress profile for DETF resonator with additional beams whose ends are (a) non-fixed, (b) fixed.

figure 6 and figure 11 it can be inferred that stress at the ends of tines is minimal in resonator FR. Thus, the novel structure comprises of a DETF resonator with additional beams having fixed ends.

Table 5 shows how the length of the additional beam impacted the vibrational mode shape of the DETF resonator. From equations (5) and (9), we can infer that the mode shape function impacts both the effective stiffness and mass of the resonator. Thus, different mode shapes will exhibit different values of mass and stiffness. In the simulations done, theoretical validation was done for resonator FR with an additional beam of 500 μm only, since it is the desired structure with least stress. The simulated results were verified analytically using equations (10-14) and were found to be in coherence with the analytical value. The generalized results of simulation are tabulated in table 6 which provides a comparison between the two additional beam structures.

Further, additional beam length with respect to tine length of the DETF resonator was investigated. The study aimed to analyse the impact on the fixed end stress of the resonator. Tine lengths were analyzed for various additional beam lengths to get optimized minimal stress values and a lower order mode for AS mode. This analysis was repeated for different tine length values. Table 7 gives the value of additional beam lengths for different tine lengths

Table 5. Impact of additional beam length on mode shape in resonator FR.

Additional beam length (μm)	AS mode shape
200	
300	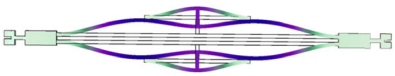
400	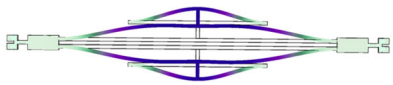
500	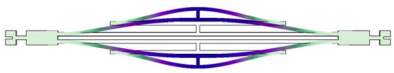
600	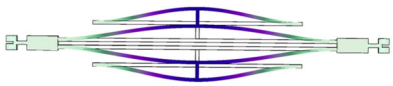

Table 6. Impact of additional beam on basic DETF resonator parameters.

Simulated parameters	Resonator NFR	Resonator FR
Additional beam length (μm)	500	500
Optimum mode	2	2
Theoretical AS mode Frequency (kHz)	84.141	268.62
Simulated AS mode Frequency (kHz)	81.278	235.96
Adjacent mode frequency (kHz)	68.663	214.65
Frequency difference between adjacent and AS mode (kHz)	12.615	21.31
Stress at fixed end (N/m^2)	15.355	0.80879

of the resonator. It can be inferred from table 7 that the stress at fixed ends was minimal for a value of additional beam length that is greater than the half of the tine length. This is because here the AS mode occurred on 2^{nd} mode position with minimum fixed end stress for each additional beam. Also, it was observed that for additional beam lengths smaller than half of tine length, the AS mode occurred as higher order mode.

5. Result discussion

In this paper first of all simulative dimensional optimization regime was followed for the existing DETF resonator designs. Then the selected design was optimised and later modified to achieve a high frequency vibrational operation for the flexural DETF resonator. The modified design was further optimised dimensionally to achieve an efficient resonator design. The results obtained are an amalgamation of simulated data and are discussed here in this section to chart out the improvisations done in DETF resonator design.

Existing DETF resonator design A6: Impact of resonator dimensions on the frequency of AS mode and its frequency difference from the adjacent nearby mode was studied. The simulations intended to reduce the stress at the fixed ends of the resonator in the lateral AS mode of vibration. Results for minimum value of stress at fixed ends along with the impact on position of occurrence of AS mode are presented based on the simulations done using COMSOL. It was observed that AS mode frequency was largely impacted by the length and width of the tine while gap along with length and width, also, affected the modal frequency difference. It was inferred that small gaps between tines should be chosen for exhibiting higher modal frequency difference. Analysis showed that stubs also aided in increasing the separation of the lateral AS mode from adjacent modes. Further, it was observed that with addition of outriggers, stress reduces in DETF resonator but with addition of stubs it reduced further. However, the addition of two-line suspension structure reduced the stress to a value approaching zero and thus produced more balanced DETF resonator. A stress value of 0.09 N/m^2 [18] and 0.87 N/m^2 [32] has been reported in literature for the basic DETF structure while a value of 0.29 N/m^2 was achieved in this study for the analysed resonator. This resonator design with minimal stress at fixed ends was henceforth selected for further modifications.

Proposed DETF resonator design FR: The basic DETF design was modified by addition of beams connected to the centre of the DETF tines via a connector beam. It was observed that though addition of beam decreased the frequency but when the ends of the additional beam were fixed, then the frequency increased drastically. From the basic design the frequency increased from 135.12 kHz to 235.96 kHz in the proposed design. The length and width of the connector and additional beams were optimized to achieve a design where stress at the fixed ends reduced to nearly zero value. A stress of nearly zero value of 0.81

Table 7. AS mode position and additional beam length with respect to DETF tine length in resonator FR.

Length (μm)		
DETF tine	Additional beam	Mode number of AS mode
500	300	2
600	420	2
700	500	2
800	500	2
900	550	2
1000	630	2

N/m^2 was achieved for the modified resonator design. Further, the stress at the ends of the tines was least for this resonator FR. The dimensional optimization also aimed to achieve lower order mode as the optimum mode. The AS mode of operation was achieved at 2^{nd} mode position in this design as well. Thus, a new DETF design is devised which is better in comparison to the basic DETF resonators. It has the advantages of considerable high frequency vibrational operation, minimal stress at the tine ends and fixed resonator ends.

Summary: Study of the optimized geometric dimensions bring into consideration certain optimization facts that can be used to design DETF resonators.

- In order to achieve the desired lateral AS mode at a lower mode position it is required that width must always be nearly half of the height of the resonator.
- Width of the stub equal to the gap between tines and outrigger width equal to half of the gap between tines aids in reducing the stress to a nearly zero value.
- For minimal stress, connector beam width should be also nearly same as tine width and its length should be double the width.
- For additional beam, the width should be same as tine width and length should be more than half of the tine length.

6. Conclusion

In order to ensure efficient operation of a resonator, it must be ensured that coupled energy from resonator into the ambient structure should be minimal. Designing of resonator is a crucial aspect to accomplish this very necessity. DETF resonators is one such design which has inherent capability of reduced energy loss. Further, high frequency operation ensures reduced energy loss but with flexural resonators, high frequency achievement is critical. A thorough numerical study was carried out for different silicon DETF resonators to obtain a balanced structure. Simulations showed that in AS vibration mode, DETF exhibited least stress at the resonator ends and hence is the optimum mode for resonator operation. The optimized balanced DETF design was further modified and then optimized to accomplish the achievement of a novel design. Optimum mode that is also desired to be positioned at a lower mode was achieved at 2nd mode position in both basic and proposed designs. With the help of incorporated modifications, frequency of the DETF design increased by around 100 kHz. Minimal stress with nearly zero value (0.29 N/m^2 for basic resonator and 0.89 N/m^2 for proposed resonator) at the tine ends was achieved through device optimization to ensure high Q factor during operation. This paper thus, proposed a new flexural DETF resonator incorporating high frequency operation in comparison to basic DETF resonator design. By simulations it was analysed that least stress was achieved during DETF vibration, when the additional beam was greater than half of tine length. Also, a theoretical vibration model for DETF resonator designs is presented and the results obtained from finite element simulation of the resonator design are validated theoretically. Further, the optimization rules obtained and demonstrated here can be of great help for designing of DETF resonators.

List of symbols

k	Effective stiffness of the resonator
M	Effective mass of the resonator
f_o	Natural resonant frequency
E	Young's modulus
ρ	Material density
F	Axial force acting upon tines
l	Length of the tine
w	Width of the tine
t	Thickness of the tine
g	Gap between tines
l_o	Outrigger width
l_f	Fixed base length
l_w	Fixed base width
l_s	Stub length
w_s	Stub width
S_l	Suspension length
S_w	Suspension width
l_a	Length of additional beam
w_a	Width of additional beam
l_c	Length of connector beam
w_c	Width of connector beam
h	Resonator height

References

[1] Petersen K, Pourahmadi F, Brown J, Parsons P, Skinner M and Tudor J 1991 Resonant beam pressure sensor fabricated with silicon fusion bonding. *TRANSDUCERS'91: IEEE International Conf. on Solid-State Sensors and Actuators. Digest of Technical Papers*, pp. 664–667

[2] Sharma A, Kumar V and Kaur H J 2022 Analysis of a micro-resonant pressure sensor with docked clamped-clamped micro-beam. In: *AIP Conference Proceedings* 2451: 020018

[3] Tai-Ran H 2008 MEMS and Microsystems: Design and Manufacture. 1st edn. McGraw Hill, New York

[4] Sharma A, Kumar V and Kaur H J 2022 Finite Element Analysis for Design Optimization of MEMS Double Ended Tuning Fork Resonator. *ECS Transactions* 107: 4697

[5] Zhang Q, Li C, Zhao Y and Zhang Z 2021 A Quartz Resonant Ultra-High Pressure Sensor With High Precision and High Stability. *IEEE Sens. J.* 21: 22553–22561

[6] Azgin K, Akin T and Valdevit L 2012 Ultrahigh-dynamic-range resonant MEMS load cells for micromechanical test frames. *J. Microelectromech Syst.* 21: 1519–1529

[7] Han D, Wang J, Yuan S, Yang T, Chen B, Teng G, Luo W, Chen Y, Li Y, Wang M and Yin Y 2019 A Mems Pressure Sensor Based on Double-Ended Tuning Fork Resonator with on-Chip Thermal Compensation. In: *20th IEEE International Conf. on Solid-State Sensors, Actuators and Microsystems & Eurosensors XXXIII (TRANSDUCERS & EUROSENSORS XXXIII)*, pp. 2061–2064

[8] Chen Y H, Li W C, Xiao X W, Yang C C and Liu C H 2019 Design optimization of a compact double-ended-tuning-fork-based resonant accelerometer for smart spindle applications. *Micromachines* 11: 42

[9] Zhang W, Zhu H and Lee J E 2015 Piezoresistive transduction in a double-ended tuning fork SOI MEMS resonator for enhanced linear electrical performance. *IEEE Trans Electron Devices* 62: 1596–1602

[10] Basu J and Bhattacharyya T K 2011 Microelectromechanical resonators for radio frequency communication applications. *Microsyst. Technol.* 17: 1557–1580

[11] Zook J D, Burns D W, Guckel H, Sniegowski J J, Engelstad R L and Feng Z 1992 Characteristics of polysilicon resonant microbeams. *Sens. Actuator A Phys.* 35: 51–59

[12] Tilmans H A, Elwenspoek M and Fluitman J H 1992 Micro resonant force gauges. *Sens. Actuator A Phys.* 30: 35–53

[13] Piazza G, Stephanou P J and Pisano A P 2006 AlN contour-mode vibrating RF MEMS for next generation wireless communications. In: *IEEE European Solid-State Device Research Conf.,* pp. 61–64

[14] Raghunathan A and Antony JK 2017 MEMS based intracranial pressure monitoring sensor. In: *2nd IEEE International Conf. on Recent Trends in Electronics, Information & Communication Technology,* pp. 451–456

[15] Sastry D V 2009 Radio Frequency Microelectromechanical Systems in Defence and Aerospace. *Def. Sci. J.* 59

[16] Vigevani G, Przybyla RJ, Yen T T, Lin C M, Guedes A, Kuypers J H, Boser B E, Horsley D A and Pisano A P 2010 Characterization of a single port aluminum nitride tuning fork. *IEEE Int. Ultrason. Symp*, pp. 1281–1285

[17] Beeby S P, Ensell G, Baker B R, Tudor M J and White N M 2000 Micromachined silicon resonant strain gauges fabricated using SOI wafer technology. *J. Microelectromech Syst.* 9: 104–111

[18] Beeby S P and Tudor M J 1995 Modelling and optimization of micromachined silicon resonators. *J. Micromech. Microeng.* 5: 103

[19] Harada K, Ikeda K, Ueda T, Kohsaka F and Isozaki K 1984 Precision transducers using mechanical resonators. tech. rep., *Yokogawa Technical Report No.*

[20] Newell W E 1968 Miniaturization of Tuning Forks: Integrated electronic circuits provide the incentive and the means for orders-of-magnitude reduction in size. *Science* 161: 1320–1326

[21] Buser R A and De Rooij N F 1989 Resonant silicon structures. *Sensors and Actuators* 17: 145–154

[22] Satchell D W and Greenwood J C 1989 A thermally-excited silicon accelerometer. *Sensors and Actuators* 17: 241–245

[23] Welham C J, Gardner J W and Greenwood J 1996 A laterally driven micromachined resonant pressure sensor. *Sens. Actuator A Phys.* 52: 86–91

[24] Welham C J, Greenwood J and Bertioli M M 1999 A high accuracy resonant pressure sensor by fusion bonding and trench etching. *Sens. Actuator A Phys.* 76: 298–304

[25] Cheshmehdoost A, Jones B E and O'Connor B 1991 Characteristics of a force transducer incorporating a mechanical DETF resonator. *Sens. Actuator A Phys.* 26: 307–312

[26] EerNisse E P and Paros J M 1983 Practical considerations for miniature quartz resonator force transducers. QUARTEX INC SALT LAKE CITY UT

[27] Clayton L D, Swanson S R and Eernisse E P 1987 Modifications of the double-ended tuning fork geometry for reduced coupling to its surroundings: finite element analysis and experiments. *IEEE Trans Ultrason Ferroelectr Freq Control* 34: 243–252

[28] Fukuzawa K, Ando T, Shibamoto M, Mitsuya Y and Zhang H 2006 Monolithically fabricated double-ended tuning-fork-based force sensor. *J. Appl. Phys.* 99: 094901

[29] Weaver W Jr, Timoshenko S P and Young D H 1991 Vibration problems in engineering. John Wiley & Sons

[30] Azgin K and Valdevit L 2013 The effects of tine coupling and geometrical imperfections on the response of DETF resonators. *J. Micromech. Microeng.* 23: 125011

[31] Cheng R, Li C, Zhao Y, Li B and Tian B 2015 A high performance micro-pressure sensor based on a double-ended quartz tuning fork and silicon diaphragm in atmospheric packaging. *Meas. Sci. Technol.* 26: 065101

[32] Shi H, Fan S and Li W 2018 Design and optimization of DETF resonator based on uncertainty analysis in a micro-accelerometer. *Microsyst. Technol.* 24: 2025–2034

[33] Roessig T A 1998 Integrated MEMS tuning fork oscillators for sensor applications. University of California, Berkeley, Doctor of Philosophy

[34] Torrents A, Azgin K I, Godfrey S W, Topalli E S, Akin T A and Valdevit L 2010 MEMS resonant load cells for micromechanical test frames: feasibility study and optimal design. *J. Micromech. Microeng.* 20: 125004

[35] Young W C, Budynas R G and Sadegh A M 2012 Roark's formulas for stress and strain. 7th edn. McGraw-Hill Education, New York

[36] Sun X, Yuan W, Qiao D, Sun M and Ren S 2016 Design and analysis of a new tuning fork structure for resonant pressure sensor. *Micromachines* 7: 148